The Origin of Outflows in Evolved Stars
Proceedings IAU Symposium No. 366, 2022
L. Decin, A. Zijlstra & C. Gielen, eds.
doi:10.1017/S1743921322000643

Outflows and disks in post-RGB objects – products of common envelope ejection?

Geetanjali Sarkar[1] **and Raghvendra Sahai**[2]

[1]Department of Physics, Indian Institute of Technology, Kanpur U.P., India
email: gsarkar@iitk.ac.in

[2]Jet Propulsion Laboratory Pasadena, CA, USA

Abstract. Interacting binaries within a common envelope, wherein the primary is a red giant are believed to result in a recently identified evolutionary class – the dusty post-RGB stars. Our SED modeling of eight post-RGBs in the LMC indicates the presence of geometrically thick disks with substantial opening angle in addition to the outer shells. We estimated the total dust mass (and gas mass assuming gas-to-dust ratio) in the disks and shells and set constraints on the dust grain compositions and sizes. The only known Galactic object of this class is the Boomerang nebula. Additionally, we present a DUSTY model of the Boomerang that can serve as a template for 2D modeling of the object using RADMC-3D. 2D modeling is essential to dissect the morphology of the spatially-unresolved post-RGBs in the LMC. These models may then be tested with future HST and ALMA imaging, together with JWST spectroscopy of these objects.

Keywords. (stars:) circumstellar matter, (stars:) binaries (including multiple): close, stars: evolution, stars: AGB and post-AGB

1. Introduction

Most proto-planetary nebulae (PPNs) are characterised by collimated bipolar lobes separated by a dusty disk or torus (Sahai et al. 1998; Kwok, Su & Hrivnak 1998; Bujarrabal et al. 1998; García-Lario, Riera & Manchado 1999; Kwok Hrivnak & Su 2000; Hrivnak et al. 2008). Following heavy mass loss on the AGB, the luminous ($L \sim 5000 - 10,000\,\mathrm{L}_\odot$), cool ($T_{eff} < 3000\,\mathrm{K}$) AGB stars are transformed into post-AGBs evolving towards higher temperatures at constant luminosity. The spherical (AGB) envelopes are transformed into aspherical bipolar/multipolar morphologies via the action of collimated high-velocity outflows that sculpt these envelopes from the inside out, as the central stars evolve to the post-AGB/PPN phase (Sahai & Trauger 1998; Sahai, Morris & Villar 2011). Phillips & Ramos-Larios 2010 and references therein have tried to explain the formation of the jet engines that produce such outflows as also the bipolar/multipolar structures in PPNe. Common envelope evolution (CEE) in close binary systems is by far the most popular amongst these.

Binarity may also be responsible for the rapid and unexpected evolution of Red Giant Branch (RGB) stars to the PPN stage (post-RGB stars). Bipolar morphology similar to post-AGB PPNe was discovered in the Boomerang Nebula (Wegner & Glass 1979; Sahai & Nyman 1997). However, the luminosity of the central star in the Boomerang is much lower ($L \sim 300\,\mathrm{L}_\odot$) than is possible for a post-AGB star. Sahai et al. (2017) show that the Boomerang is most likely a post-RGB star and that merger with a binary companion may have triggered its extreme mass loss ($\sim 10^{-3}$ $\mathrm{M}_\odot \mathrm{yr}^{-1}$) at a very high ejection velocity (165 $\mathrm{km\,s}^{-1}$), over a relatively short period (3500 yr) via CEE.

Using optical spectroscopy and *Spitzer* photometry, Kamath et al. (2014, 2015, 2016) identified post-RGB objects similar to the Boomerang in the Large and Small Magellanic Clouds (LMC and SMC). These objects were found to have large mid-IR excesses. Distance modulus for the LMC/18.54 and SMC/18.93 (Keller & Wood 2006) enabled reliable luminosity estimates for these stars; the low luminosities (< 2500 $L_\odot$) indicate that these stars have not yet reached the AGB phase. Post-RGB stars are thus separated from post-AGB ones by their low luminosities.

2. Post-RGB stars in the LMC

We selected a sample of eight post-RGB stars in the LMC with mid and far-IR excess from Kamath et al. (2015: hereafter KWVW15). Our sample consists of an equal number of "shell" (dust peak beyond 10 μm) and "disk" (peak around 10 μm or bluer) sources from KWVW15. On a colour-colour plot, the shell sources have $[3.6]-[4.5] < 0.5$ and $[8]-[24] > 4.0$. Disk sources, on the other hand, have $[3.6]-[4.5] > 0.5$, or in some cases, $[3.6]-[4.5] < 0.5$ in combination with $[8]-[24] < 3.0$. Additionally, to ensure that the objects are indeed post-RGB (and not post-AGB) we selected objects with $L < 1000$ $L_\odot$. The observed SEDs extend from the U-band to 24μm.

The SEDs were modeled using the one-dimensional radiative transfer code, DUSTY (Ivezić et al. 2012) (Fig. 1, Table 1). The dust density was assumed to be proportional to r^{-2}, where r is the radial distance from the star. Whenever a single shell model (one-component model) was found to be insufficient to obtain a fit to the observed SED, we used a two-component fit, in which we added an inner component, representative of a hot, compact disk. We approximated the inner disk to be an axially symmetric wedge-shaped fraction of a sphere; this fraction is hereafter referred to as the "disk fraction"†. The free parameters for the modeling include the dust temperature (T_d at the inner boundary of the disks/shells, the dust grain sizes, grain composition, optical depth (τ) at 0.55μm and relative shell (disk) thickness (Y = ratio of the outer to the inner shell/disk radius).

The DUSTY code outputs the SED, normalized to the bolometric flux, F_{bol}, which was determined by scaling the model SED to match the de-reddened SED of each source. We estimated the luminosity for each model as $L = 4\pi d^2 F_{bol}$, assuming a distance, d=50 kpc, for the LMC. The dust mass M_d in the circumstellar component is estimated using:

$$M_d = 4\pi R_{in}^2 Y(\tau_{100}/\kappa_{100})$$

that applies to objects obeying a r^{-2} density distribution; the total mass (gas+dust), $M_{gd} = M_d\delta$ (Sarkar & Sahai 2006). R_{in} is the inner radius of the dust shell, Y is the shell relative thickness specified in the DUSTY input (R_{out}/R_{in}), τ_{100} is the shell optical depth at 100 μm, κ_{100} is the dust mass absorption coefficient at 100 μm and δ is the gas-to-dust ratio. We assume $\delta = 200$, and $\kappa_{100} = 34\,cm^2g^{-1}$, as in (Sarkar & Sahai 2006). The derived parameters from our best-fit models are summarised in Table 1. For comparison, we show our model dust mass values, M_d(outer shell), overplotted (horizontal lines, Fig. 2) on a plot of theoretically estimated dust masses in the ejecta of common envelope systems versus initial stellar mass, taken from Fig. 2 of Lü et al. (2013).

3. Dissecting post-RGB morphology using RADMC-3D

Not much is known about the as yet unresolved dusty post-RGBs in the LMC and SMC. We may dissect their morphology by using the code RADMC-3D (Dullemond et al. 2012). Using the latter, observed SEDs of the post-RGBs may be modeled to estimate the

† A disk with an opening angle of θ°, intercepts a fraction $\sin(\theta)$ of the radiation emitted by the star within a 4π solid angle.

https://doi.org/10.1017/S1743921322000643 Published online by Cambridge University Press

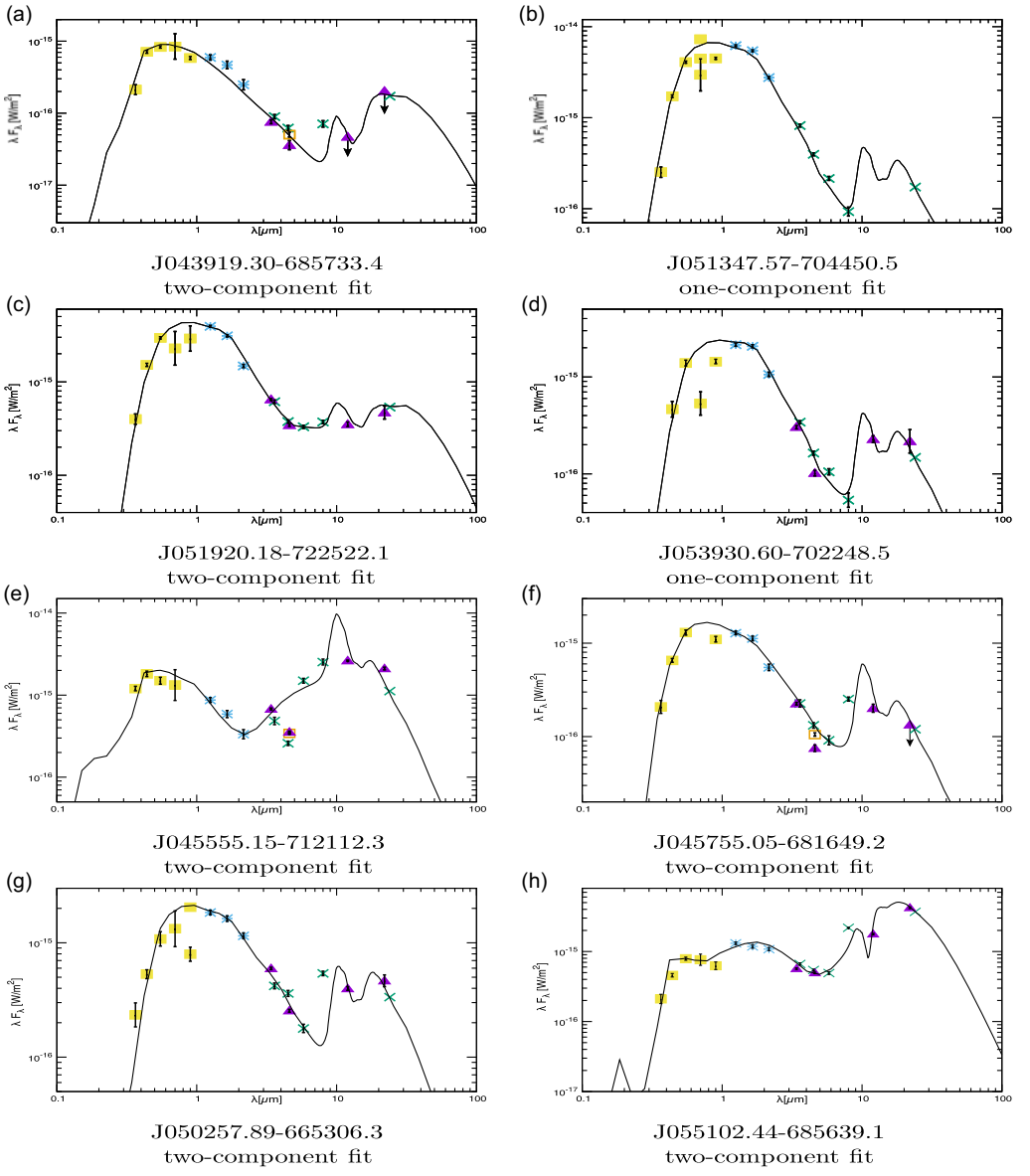

Figure 1. The best-fit models (black curves) to the observed SEDs of the post-RGB sources. The observed fluxes are de-reddened for Galactic and LMC reddening. U,B,V,R,I (yellow), 2MASS J,H,K (cyan) data are plotted along with WISE photometry (purple) and data from the SAGE-LMC Survey (green) which covers the IRAC and MIPS bands. The error bars and upper limits (arrows) are indicated in black.

disk mass, the flaring angle of the disk, the grain sizes in the disk, the disk inclinations, the disk scale height (when the the inclinations are closer to face-on) and the extent of the disk. We can then produce 2D-images of the objects at a particular wavelength for comparison with future HST and ALMA images. This approach may be tested using the well-studied Boomerang nebula in our Galaxy as a template.

ALMA images of the Boomerang (Sahai et al. 2017) revealed three distinct components in its morphology – compact disk, circumstellar envelope and bipolar lobes.

https://doi.org/10.1017/S1743921322000643 Published online by Cambridge University Press

Table 1. Important parameters derived from the best-fit pRGB models.

Object	Inner disk					Outer shell					
	T_d^a(in) (K)	τ^b	a_{min}^c (μm)	a_{max}^d (μm)	M_{gd}^e ($M_\odot$)	T_d^a(in) (K)	τ^b	a_{min}^c (μm)	a_{max}^d (μm)	M_{gd}^e ($M_\odot$)	L^f ($L_\odot$)
shell sources											
J043919.30-685733.4	1000	0.5	0.005	0.25	2.19×10^{-8}	130	0.65	0.005	0.25	5.2×10^{-3}	116
J051347.57-704450.5	...	...	...	...	...	250	0.35	0.1	0.25	4×10^{-5}	776
J051920.18-722522.1	500	0.4	0.3	20	2.59×10^{-5}	110	0.65	0.005	0.25	3.44×10^{-2}	582
J053930.60-702248.5	...	...	...	...	...	300	0.70	0.005	0.25	5.81×10^{-5}	295
disk sources											
J045555.15-712112.3	800	0.7	0.005	0.25	2.67×10^{-6}	500	1.8	0.005	0.25	8.73×10^{-5}	621
J045755.05-681649.2	1300	0.5	0.005	2.0	9.64×10^{-9}	400	0.6	0.1	1.0	5.73×10^{-5}	217
J050257.89-665306.3	1200	0.5	0.3	5.0	5.77×10^{-8}	250	0.75	0.005	1.0	2.68×10^{-4}	303
J055102.44-685639.1	2000	1.0	0.005	0.05	1.99×10^{-8}	350	12.0	0.005	0.07	3.05×10^{-3}	621

a: The (input) dust temperature at shell (disk) inner radius; **b:** The dust shell's (disk's) optical depth at 0.55μ; **c:** The minimum dust grain size; **d:** The maximum dust grain size; **e:** The (inferred) circumstellar (gas+dust) mass ($M_{gd} = M_d\delta$); **f:** The (inferred) luminosity

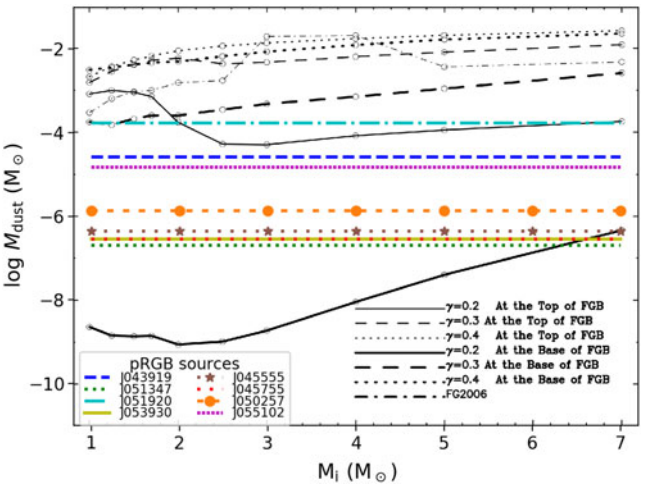

Figure 2. The circumstellar dust mass (M_d) of our post-RGB objects are shown (horizontal lines) on a plot of theoretically estimated dust masses in the ejecta of common envelope systems versus initial stellar mass, taken from Fig. 2 of Lü et al. (2013). FGB refers to the first red giant branch. FG2006 refers to results by Ferrarotti & Gail (2006), showing the dust masses produced in the dust-driven outflows of AGB stars.

We reconstructed its SED from the U-band to 140μm using the Vizier database (https://vizier.u-strasbg.fr/viz-bin/VizieR). A DUSTY model fit to the SED (Fig. 3) required an inner disk, a warm inner shell and an utra-cold outer shell in agreement with Sahai et al. (2017). The values of the physical parameters chararacterizing the model components are given in Table 2; these parameters will provide initial estimates for the 2D modeling of the object using RADMC-3D.

4. Discussion

When the primary in a binary system overflows its Roche lobe and the resulting mass transfer proceeds too rapidly to be accreted by the compact companion, a CE system results. CEE (Paczynski 1976; Ivanova et al. 2013) may give rise to close binary systems. Two scenarios may exist — a rapid plunge in of the companion or a slow spiral-in

https://doi.org/10.1017/S1743921322000643 Published online by Cambridge University Press

Table 2. Model of the Boomerang Nebula.

Component	Parameter	Value
Cool Shell	R_{in}	6.52×10^{16}cm
	Y	20
	T_d(in)	50 K
	τ	4.0
	grain size	$0.1 - 0.25\,\mu$m
	M_d	$3.26 \times 10^{-2} M_\odot$
Warm Shell	R_{in}	3.23×10^{16}cm
	Y	1.5
	T_d(in)	145 K
	τ	1.0
	grain size	MRN
	M_d	$2.85 \times 10^{-4} M_\odot$
Inner Disk	R_{in}	6.08×10^{14}cm
	Y	1.5
	T_d(in)	1100 K
	τ	40.0
	grain size	MRN
	M_d	$4.03 \times 10^{-6} M_\odot$

R_{in}=inner radius of dust shell(disk); Y=thickness of dust shell (disk); T_d=dust temperature at inner shell (disk) boundary; τ=optical depth at 0.55μm; MRN: Mathis, Rumpl, Nordsieck grain size distribution (Mathis et al. 1977); M_d=circumstellar dust mass

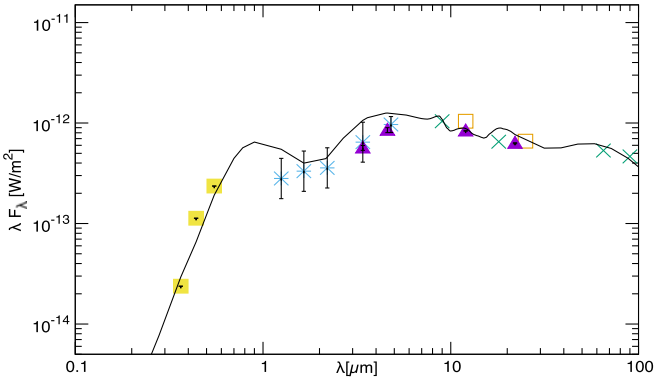

Figure 3. DUSTY model fit (black) to the observed SED of the Boomerang nebula (disk fraction = 0.5). The observed fluxes are de-reddened using $A_v = 0.28$. U,B,V (yellow), J,H,K,L,M (blue) data are plotted along with IRAS fluxes (orange), WISE photometry (purple) and AKARI data (green). The error bars are indicated in black. The Boomerang is assumed to be at a distance of 1.5 kpc (Sahai & Nyman 1997).

phase. In the former, if enough orbital energy is deposited to the CE via dynamical friction, the whole envelope is ejected on a dynamical timescale (Paczynski 1976). The second case provides an alternate route for the envelope ejection (Ivanova et al. 2002; Podsiadlowski et al. 2010) over "several dynamical time scales" (Ivanova et al. 2013; Clayton et al. 2017). Recently, a third scenario has been proposed by Glanz & Perets (2018) wherein dust driven winds similar to those observed in AGB stars may lead to the ejection of the CE.

Dust formation may occur in the expanding gas (Lü et al. 2013, Iaconi et al. 2020) which may explain the presence of circumstellar dust shells in these systems. Some fraction of the ejected mass may also fall back and interact with the binary leading to the formation

https://doi.org/10.1017/S1743921322000643 Published online by Cambridge University Press

of circumbinary disks (Kashi & Soker 2011). Our derived dust masses may be taken as a lower limit since a substantial mass may lie longwards of 24μm. Comparison of our model dust shell masses with theoretical models of Lü et al. (2013) (Fig. 2) suggests that CEE occurred near or at the tip of the RGB. Further, we find that the disk fractions are surprisingly large (typically 0.3–0.4), implying that these are geometrically thick, flared structures with a substantial opening angle. Our modeling shows that the KWVW15 "shell"/"disk" classification is not robust. All "disk" sources in our sample require the presence of "shells". In addition, we find the presence of a disk in some "shell" sources (J043919.30-685733.4 and J051920.18-722522.1). We also find evidence that for some post-RGB sources the ejected matter may be carbon-rich, even though it is expected to be oxygen-rich. This provides independent support for the hypothesis of binary interaction leading to the formation of dusty post-RGBs. Modeling the unresolved post-RGBs using RADMC-3D will pave the way for future observations with HST, JWST, and ALMA that will lead to a better understanding of the evolutionary processes that produce post-RGB objects.

Acknowledgements

G.S. would like to acknowledge financial support from the Department of Science and Technology (DST), Government of India, through a grant numbered SR/WOS-A/PM-93/2017. R.S.'s contribution to the research described here was carried out at the Jet Propulsion Laboratory, California Institute of Technology, under a contract with NASA, and funded in part by NASA via ADAP awards, and multiple HST GO awards from the Space Telescope Science Institute.

References

Bujarrabal, V., Alcolea, J., Sahai, R., Zamorano, J. & Zijlstra, A. A. 1998, *A&A*, 331, 361
Clayton, M., Podsiadlowski, P., Ivanova, N., Justham, S. 2017, *MNRAS*, 470, 1788
Dullemond, C. P., Juhasz, A., Pohl, A., et al. 2012, *RADMC-3D: A multi-purpose radiative transfer tool, Astrophysics Source Code Library*. http://ascl.net/1202.015
García-Lario, P., Riera, A. & Manchado, A. 1999, *ApJ*, 526, 854
Glanz, H. & Perets, H.B. 2018, *MNRAS*, 478, L12
Hrivnak, B. J., Smith, N., Su, K. Y. L. & Sahai, R. 2008, *ApJ*, 688, 327
Iaconi, R., Maeda, K., Nozawa, T., De Marco, O., Reichardt, T., 2020, *MNRAS*, 497, 3
Ivanova, N., Podsiadlowski, P., Spruit, H. 2002, *MNRAS*, 334, 819
Ivanova, N., Justham, S., Chen, X., et al. 2013, *The Astronomy and Astrophysics Review*, 21, 59
Ivezić, Z., Nenkova, M., Heymann, F. & Elitzur, M. 2012, *U*ser Manual for DUSTY (V4)
Kamath, D., Wood, P. R. & Van Winckel, H. 2014, *MNRAS*, 439, 2211
Kamath, D., Wood, P. R. & Van Winckel, H. 2015, *MNRAS*, 454, 1468
Kamath, D., Wood, P. R., Van Winckel, H., & Nie, J.D. 2016, *A&A* (Letters), 586, L5
Kashi, Amit & Soker, Noam 2011, *MNRAS*, 417, 1466
Keller S. C. & Wood P. R. 2006, *ApJ*, 642, 834
Kwok, S., Su, K. Y. L. & Hrivnak, B. J. 1998, *ApJ* (Letters), 501, L117
Kwok, S., Hrivnak, B. J., & Su, K. Y. L. 2000, *ApJ* (Letters), 544, L149
Lü, G., Zhu, C. & Podsiadlowski, P. 2013, *ApJ*, 768, 193
Mathis, J. S., Rumpl, W. & Nordsieck, K. H. 1977, *ApJ*, 217, 425
Paczynski, B. 1976, in *I*AU Symposium 73, *Structure and Evolution of Close Binary Systems*, eds. Eggleton, P., Mitton, S., Whelan, J., p. 75
Phillips, J. P., Ramos-Larios, G. 2010, *MNRAS*, 405, 2179
Podsiadlowski, P., Ivanova, N., Justham, S., Rappaport, S. 2010, *MNRAS*, 406, 840
Sahai, R. & Nyman, Lars-Ake 1997 *ApJ*, 487, L155

Sahai, R., et al. 1998, *ApJ*, 493, 301
Sahai, R. & Trauger, J. T. 1998, *AJ*, 116, 1357
Sahai, R., Morris, M. R. & Villar, G. G. 2011, *AJ*, 141, 134
Sahai, R., Vlemmings, W.H.T. & Nyman, L.A. 2017, *ApJ*, 841, 110
Sarkar, G. & Sahai, R. 2006, *ApJ*, 644, 1171
Wegner, G. & Glass, I. S. 1979, *MNRAS*, 188, 327

https://doi.org/10.1017/S1743921322000643 Published online by Cambridge University Press